

Inverse estimation of soil hydraulic properties and water repellency following artificially induced drought stress

Vilim Filipović^{1*}, Thomas Weninger², Lana Filipović¹, Andreas Schwen³, Keith L. Bristow⁴, Sophie Zechmeister-Boltenstern⁵, Sonja Leitner⁵

¹ University of Zagreb, Faculty of Agriculture, Department of Soil Amelioration, Svetošimunska 25, 10000 Zagreb, Croatia.

² University of Natural Resources and Life Sciences Vienna (BOKU), Institute of Hydraulics and Rural Water Management, Muthgasse 18, 1190 Vienna, Austria.

³ Austrian Agency for Health and Food Safety (AGES), Institute for Plant Protection Products, Spargelfeldstraße 191, 1220 Vienna, Austria.

⁴ CSIRO Agriculture & Food, PMB Aitkenvale, Townsville, QLD 4814, Australia.

⁵ University of Natural Resources and Life Sciences Vienna (BOKU), Institute of Soil Research, Peter-Jordan-Straße 82, 1190 Vienna, Austria.

* Corresponding author. Tel.: 00385 1 2393711. E-mail: vfilipovic@agr.hr

Abstract: Global climate change is projected to continue and result in prolonged and more intense droughts, which can increase soil water repellency (SWR). To be able to estimate the consequences of SWR on vadose zone hydrology, it is important to determine soil hydraulic properties (SHP). Sequential modeling using HYDRUS (2D/3D) was performed on an experimental field site with artificially imposed drought scenarios (moderately M and severely S stressed) and a control plot. First, inverse modeling was performed for SHP estimation based on water and ethanol infiltration experimental data, followed by model validation on one selected irrigation event. Finally, hillslope modeling was performed to assess water balance for 2014. Results suggest that prolonged dry periods can increase soil water repellency. Inverse modeling was successfully performed for infiltrating liquids, water and ethanol, with R^2 and model efficiency (E) values both > 0.9 . SHP derived from the ethanol measurements showed large differences in van Genuchten-Mualem (VGM) parameters for the M and S plots compared to water infiltration experiments. SWR resulted in large saturated hydraulic conductivity (K_s) decrease on the M and S scenarios. After validation of SHP on water content measurements during a selected irrigation event, one year simulations (2014) showed that water repellency increases surface runoff in non-structured soils at hillslopes.

Keywords: Inverse modeling; Water and ethanol infiltration; SHP estimation; Water dynamics; HYDRUS (2D/3D).

INTRODUCTION

Soil water repellency (SWR) is a reduction in the rate of wetting and retention of water in soil caused by drying and the presence of various hydrophobic coatings on soil particles. The physical background is not yet fully understood, but it is widely accepted that this phenomenon is most likely caused by water-repellent compounds that can coat soil mineral particles or be present as interstitial matter in soil pores (Doerr et al., 2000). SWR can increase substantially due to seasonal events, e.g. drought periods and/or wildfires (Jordan et al., 2013; Schwen et al., 2015). With the projected continuation of climate change, frequency and severity of drought events will intensify in most regions of the globe and the relevance of SWR effect on soil water dynamics is expected to increase in the future (Fischer and Knutt, 2014; Stocker et al., 2013).

SWR is not a stationary soil property but highly variable over time, depending on soil water content. Generally, SWR increases with decreasing water content (Jordan et al., 2013). Furthermore, although dry soils may be very water repellent initially, the repellency effect can disappear after prolonged contact with water. The duration of this process is described as repellency persistence. Besides persistence, SWR is also defined by severity of repellency, both of which can be expressed quantitatively (Chau et al., 2014). The intensity of SWR is characterized by the contact angle between soil surface and infiltrating water (Subedi et al., 2013). Hydrophobic conditions are present if contact angle above 90° is present, however even the contact angle in between 0° and 90° can affect water infil-

tration (Hallett et al., 2001). The SWR cannot be measured directly as physical value in the field, but has to be obtained indirectly, e.g. by observing the difference in flow behavior between water and fully-wetting fluid. Due to specific physico-chemical properties of ethanol (i.e. lower surface tension), ethanol is considered to be complete wetting fluid which is commonly used in SWR estimation (i.e. zero repellency; Lamarter et al., 2010; Watson and Letey, 1970). Further established methods (laboratory) are based on the influence which SWR has on other soil physical parameters, e.g. contact angle between water and soil surface, water drop penetration time, or capillary effect (Letey et al., 2000; Shang et al., 2008).

In comparison to non-repellent soils, water repellent soils have different infiltration patterns (initially postponed infiltration which increases after contact angle between water and soil particles decreases e.g. Bughici and Wallach, 2016; Debanò, 1975) and increased fractions of preferential flow (e.g. Ritsema et al., 1993; 2000) or surface runoff (Lemnitz et al., 2008). Soil infiltration experiments with a KBr tracer performed by Clothier et al. (2000) demonstrated (i) transient behavior of fingered preferential flow during the breakdown of hydrophobicity as a result of increasing soil water content, and (ii) solute penetration of the whole soil pore space after complete wetting. Hence, SWR appears to be reversible and very dynamic in time and space, thus making it difficult to predict. In a review by Jordan et al. (2013) the authors show that the majority of previous SWR studies are focused on the relationship between SWR and different soil properties (texture, organic matter content, soil chemical characteristics) or microbiological activity as a

response to soil management. However, SWR dynamics under different climatic scenarios and how it can affect soil moisture in the long term remains unclear.

To assess the water dynamics under various field conditions as well as for predictions of future scenarios, modeling has proven to be an appropriate tool (Šimůnek et al., 2016; Vereecken et al., 2016). However, in available modeling software applications for plot or profile scale SWR is not accounted for as a separate parameter, but may be preferably expressed during the procedure of soil hydraulic properties (SHP) estimation. Several studies highlight that the influence of SWR on SHP is evident in the hysteresis effect (Bauters et al., 1998; Czachor et al., 2010). Generally, the hysteresis is highly related to SWR, and the SWR effect is primarily detectable on the wetting curve (Hardie et al., 2013; Stoffregen and Wessolek, 2014). In a laboratory study focusing on SWR-influenced SHP, Diamantopoulos et al. (2013) performed multistep inflow/outflow experiments with water and ethanol on four substrates, where they gradually induced water repellency by adding water repellent material (hydrophobic sand) in different ratios to soil. The experiments were performed with initially dry or initially saturated conditions to account for hysteresis, and inverse parameter estimation was performed to obtain SHP. Their results showed that SWR affects SHP on the wetting curve, contributing to the hysteresis effect, and that the artificial mixtures with a higher fraction of water repellent substances had a larger effect of SWR on SHP compared to naturally repellent soils. Therefore, during SHP estimation in water repellent soils, it is important to account for the most severe SWR effects expected during the initial soil wetting process (infiltration).

Hysteretic forms of SHP are sometimes implemented in modeling applications to account for SWR, e.g. Nieber et al. (2000) simulated infiltration in wettable and water repellent sand with a 2D finite-element model where SWR was taken into account by including hysteresis in the water retention curve and two slightly different equations for the unsaturated hydraulic conductivity function. Ganz et al. (2014) modeled water infiltration patterns in water repellent soils as well, but using a 3D-simulation in HYDRUS (2D/3D). They emphasized a strong need for the inclusion of hysteresis (model implemented in HYDRUS by Lenhard and Parker, 1992) and a scaling procedure based on independently measured contact angle data (method by Bachmann et al., 2007).

To investigate the impact of different rainfall distribution patterns on soil water dynamics, modeling using data from an artificially induced drought stress field experiment was performed in order to investigate the full effect of SWR on the hysteretic wetting curve. The objective of this study was (i) to estimate SHP from disc infiltrometer experiments with water and ethanol using inverse modeling approach and (ii) to further assess the impact of different artificially induced drought scenarios on SWR and consequently on local vadose zone hydrology using HYDRUS (2D/3D).

MATERIALS AND METHODS

Field site description

The experimental field was set up at the iLTER-site (International Long Term Ecological Research) in the Rosalian Mountains, Austria (47°42'26.33" N, 16°17'54.5" E, 600 m a.s.l.; Leitner et al., 2017). The mean annual temperature is 6.5°C and the mean annual precipitation is 796 mm at this location. The experimental site was situated in a forested hillslope with mature beech trees (*Fagus sylvatica* L.) and no understory on a plateau with a sloping angle of 16°. The soil type was classified

as Podsolc Cambisol according to the WRB (World reference base for soil resources, IUSS, 2014) covering impermeable granitic bedrock at 75–80 cm below the soil surface following the hillslope curvature. The soil profile was covered with an organic matter O horizon (0–7 cm), followed by an eluvial humus Aeh-horizon (7–25 cm), a cambic, slightly humusos-oxoquioxidic Bhs-horizon (25–50 cm) over weathered granitic rock debris (C-horizon 50–75 cm) (Schwen et al., 2014). To assess the impact of changed rainfall distribution patterns on various soil properties, this experimental trial was established in 2013 (Leitner et al., 2017). Briefly, two artificially induced drought stress scenarios were applied during the vegetation period (May–October): a moderately (M) stressed scenario which had six consecutive cycles of four weeks drying followed by an intensive 75 mm irrigation, and a severely (S) stressed scenario which had three cycles of eight weeks drying followed by a larger irrigation event with 150 mm of irrigation. Stressed plots were protected from natural rainfall during vegetation periods by a plastic roof 1.20 m above the soil surface (each treatment having 4 plots, 2 m × 2 m, Fig. 1). Plots were irrigated with sprinkler irrigation systems with axial-flow full cone nozzles (Series 460, Lechler GmbH) installed under the roofs using descaled tap water from a nearby field station. The duration of the irrigation events were 2h each. To be able to compare the results with natural conditions, four control plots (C) received only natural rainfall. Drought plots had additional trenches (20 cm deep) at the upper end of the plot to avoid any lateral flow and/or surface runoff from elevated ground to enter the plots. In each plot, soil volumetric water content was measured at 10 cm depth in the Aeh horizon (VWC, TDR theta ML2x probes, UMS, Germany), with measurement intervals of 30 minutes. Climatic data were collected from a meteorological station located 500 m from the field site and used to calculate evapotranspiration according to Penman-Monteith (Monteith, 1981).

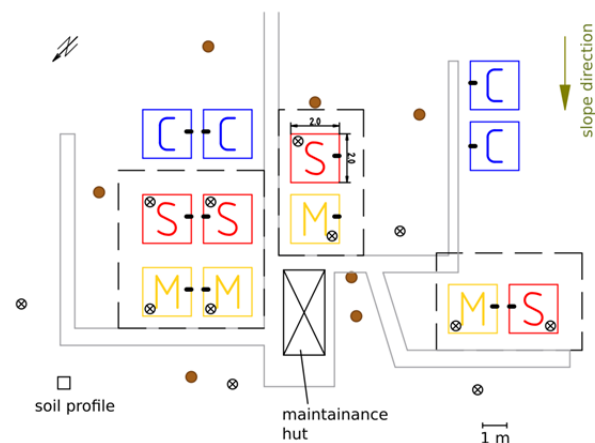


Fig. 1. iLTER experimental site scheme with bold lines as bridge pathways, dashed lines as plot roofs, colored squares as experimental units (2 × 2 m), black bold dashes as TDR-probes, X-ed circles as locations of performed infiltration experiments and brown points as trees. C stands for control, M for moderate, and S for severe stress. Infiltration experiments for control areas in Schwen et al. (2015) were conducted outside of the equipped squares to minimize influences to the soil system, especially to soil biology by ethanol.

Measurements of soil hydraulic parameters

Infiltration experiments were performed during September 2014 in all three scenarios (M, S, and C) in four repetitions as described elsewhere (Schwen et al., 2014, 2015) using a self-

Table 1. Basic soil physical properties at the iLTER experimental site (Austria) for Podsolc Cambisol soil profile: clay, silt and sand fraction, total porosity ϕ , bulk density ρ_b , and soil organic carbon (OC) content, Values were derived from a soil profile where samples were taken from incremental 5-cm-layers (uppermost sample from depth = 0–5cm), averaged for soil horizons (standard deviation in brackets). More detailed in Schwen et al., 2014, Fig. 1(b).

Horizon	Depth	Clay	Silt	Sand	OC	Porosity, ϕ	Bulk density, ρ_b
	cm	g g^{-1}	g g^{-1}	g g^{-1}	g g^{-1}	$\text{cm}^3 \text{cm}^{-3}$	g cm^{-3}
O	0–7	0.120 (–)	0.520 (–)	0.360 (–)	0.051 (–)	0.630 (–)	0.980 (–)
Aeh	7–25	0.090 (0.0125)	0.252 (0.0343)	0.659 (0.0438)	0.016 (0.0095)	0.510 (0.0326)	1.300 (0.0941)
Bhs	25–50	0.088 (0.0092)	0.240 (0.0524)	0.673 (0.0611)	0.002 (0.0027)	0.428 (0.0268)	1.516 (0.0712)
C	50–75	0.083 (0.0382)	0.191 (0.0204)	0.726 (0.0565)	0.000 (–)	0.378 (0.0164)	1.644 (0.0391)

constructed tension disc glass infiltrometer which allowed using both water and ethanol as infiltrating liquids (Schwen et al., 2015). These data served as an input for SHP estimation using inverse modeling (the procedure is explained in the next section). Before the infiltration measurements were made, the organic litter was removed to ensure that the measurements were performed at the top of the mineral Aeh horizon. Additionally, a thin layer of uniform glass beads was used at the soil surface to ensure good contact between soil and the porous disc (Dragonite, Jaygo Inc.; diameter: 0.45 mm). Infiltration measurements (water and ethanol) were conducted using different pressure heads (e.g., –10, –5, –3, –1 cm), in four replicates (one per plot) with each liquid. At the end of the water infiltration, the soil was covered to prevent any physical disturbance. Two days later, infiltration experiments were performed at the same specific spots using ethanol as the infiltration liquid with the glass beads layer replaced where necessary. Differences in the dynamic viscosity (η) of water ($\eta = 1.0$ mPa) and ethanol ($\eta = 1.2$ mPa) results in different liquid infiltration rates, even at identical liquid contents. To be able to compare the two infiltration experiments, the infiltration rates of ethanol were corrected for the difference in viscosity between water and ethanol using a factor of 1.2 (Jarvis et al., 2008). Considering different physicochemical properties of water and ethanol, the ethanol pressure head values were scaled based on the capillary rise equation which takes into account the difference between surface tension and density of particular liquids:

$$h_i = \frac{2\sigma_i \cos\gamma}{r\rho_i g} \quad (1)$$

where σ is the surface tension (mN m^{-1}), γ is the contact angle ($^\circ$), r is the equivalent capillary radius (m), ρ is the density of the liquid (g cm^{-3}), and g is the acceleration due to gravity (m s^{-2}). The subscript i refers to water (w) or ethanol (e). With the water and ethanol surface tension at 20°C of 72.7 mN m^{-1} and 22.4 mN m^{-1} , and a density of 0.998 g cm^{-3} and 0.789 g cm^{-3} , respectively, a correction factor between h_e and h_w of 2.5 was assumed (Diamantopoulos et al., 2013; Lamparter et al., 2010). Multiplying h_e with 2.5 results in the effective supply pressure ($h_{e, \text{eff}}$) giving the applied ethanol pressure heads of –25, –12.5, –7.5, and –2.5 cm. The correction factor assumes that the contact angles of water/ethanol and soil surface are identical ($\gamma_e = \gamma_w$), despite the fact that water contact angle in the field was oscillating in time. However, the differences in the contact angle reflect SWR through the different infiltration volumes for each liquid and consequently inversely estimated SHP. Initial water content was determined using the gravimetric method on

undisturbed soil cores of 250 cm^3 volume ($n = 4$ per treatment). Average initial water content values were 0.17, 0.19, and 0.31 $\text{cm}^3 \text{cm}^{-3}$ for M, S and C treatments prior to the water infiltration experiments. The same water contents were assumed to be present prior to ethanol infiltration experiments (no additional sampling/measurements were done in order to prevent disruption of the infiltration spots). Using the same soil core samples, SHP were estimated using the evaporation method (Schindler et al., 2010; device: HYPROP, UMS GmbH, Munich, Germany). Although SHP was measured by the evaporation method, only part of the measured data was used to obtain certain hydraulic parameters (porosity, θ_s) while the rest of the curve fitting was performed using inverse modeling based on the data from the infiltration experiments. SWR tend to be more expressed in drier soils and decreases with increased soil moisture (Dekker and Ritsema, 1994; Diamantopoloulos et al., 2013; Liu et al., 2012), thus starting with initially dried soil and performing infiltration experiments to investigate SWR in different treatments seemed appropriate. Particle size distribution was determined by a combination of sieving and sedimentation experiments according to Gee and Or (2002). Basic soil physical properties for the iLTER experimental site are given in Table 1.

Numerical modeling

Numerical modeling was performed with the HYDRUS (2D/3D) model (Šimůnek et al., 2016) using a three-step simulation process:

1. Inverse modeling based on water and ethanol field infiltration data – to obtain SHP;
2. Simulation of a particular irrigation event using obtained SHP – to validate the model using field TDR measurements;
3. Seasonal simulation (2014) – to assess the effect of SWR on water dynamics in hillslope areas.

This approach is explained in more detail in the following sections.

Inverse modeling to estimate soil hydraulic properties

Tension disc infiltration measurement data (average of four repetitions) with water and ethanol for the S, M, and C plots (Schwen et al., 2015) were used to obtain SHP using inverse modeling (Hopmans et al., 2002). A numerical solution of the Richards' equation coupled with the Levenberg-Marquardt nonlinear minimization method implemented in the HYDRUS (2D/3D) model was used. The program solves the equation numerically using a quasi-three-dimensional axisymmetric finite element code. The Richards' equation, which describes isothermal Darcian flow in a variably saturated rigid porous

medium, is used in the model in its modified form (Šimůnek et al., 1998):

$$\frac{\partial \theta}{\partial t} = \frac{1}{r} \frac{\partial}{\partial r} \left(rK \frac{\partial h}{\partial r} \right) + \frac{\partial}{\partial z} \left(K \frac{\partial h}{\partial z} \right) + \frac{\partial K}{\partial z} \quad (2)$$

where θ is the volumetric water content [$L^3 L^{-3}$], h is the pressure head [L], K is the unsaturated hydraulic conductivity [$L T^{-1}$], r is a radial coordinate [L], z is vertical coordinate [L], positive upwards, and t is time [L]. Equation (2) was solved numerically for the following initial and boundary conditions which reflect the initial and boundary conditions of the tension disc infiltrometer experiment:

$$\theta(r, z, t) = \theta_i \quad t = 0 \quad (3)$$

$$h(r, z, t) = h_0 \quad 0 < r < r_0, z = 0 \quad (4)$$

$$\frac{\partial h(r, z, t)}{\partial z} = -1 \quad r > r_0, z = 0 \quad (5)$$

$$h(r, z, t) = h_i \quad r^2 + z^2 \rightarrow \infty \quad (6)$$

where θ_i is the initial soil water content [$L^3 L^{-3}$], h_0 is the time-variable supply pressure head imposed by the tension disc infiltrometer for water (-10, -5, -3, -1 cm) and ethanol (-25, -12.5, -7.5, -2.5 cm) [L], and r_0 is the disc radius (porous disc radius of 2.9 cm) [L]. The SHP, estimated from ethanol infiltration volumes (scaled to match water physicochemical properties), were assumed to reflect the water infiltration in hydrophilic soil.

Soil hydraulic functions $\theta(h)$ and $K(h)$ used in the inverse and direct simulations (next section) were described using the van Genuchten-Mualem model (VGM, van Genuchten, 1980) defined as follows:

$$\theta(h) = \theta_r + \frac{\theta_s - \theta_r}{(1 + |\alpha h|^n)^m} \quad \text{for } h < 0 \quad (7)$$

$$\theta(h) = \theta_s \quad \text{for } h \geq 0$$

$$K(h) = K_s S_e^l \left(1 - \left(1 - S_e^m \right)^{\frac{1}{m}} \right)^2 \quad (8)$$

$$S_e = \frac{\theta - \theta_r}{\theta_s - \theta_r} \quad (9)$$

$$m = 1 - \frac{1}{n}; \quad n > 1 \quad (10)$$

where θ_r and θ_s denote residual and saturated volumetric water content [$L^3 L^{-3}$], respectively, K_s is the saturated hydraulic conductivity [$L T^{-1}$], S_e is the effective saturation [-], α [L^{-1}] and n [-] are shape parameters, and l [-] is a pore connectivity parameter. Pore connectivity parameter (l) was fixed to 0.5 as recommended by Mualem et al., (1976) to avoid optimization of large number of parameters. Please note that the initial condition was given in terms of the soil water content (values presented in field site description chapter). Šimůnek and van Genuchten (1997) showed that, compared to the use of pressure

head, providing initial condition in this form ensures a more stable and unique solution of the inverse problem. Soil surface boundary conditions below the disc infiltrometer and the remaining soil surface are represented by Eqs. 4 and 5, respectively. Eq. 6 assumes that all subsurface boundaries are distant from the supply source and do not influence the results in any way. The inverse solution was obtained using a combination of cumulative infiltration data and observed initial/final water content after minimization of the objective function. The simulated axisymmetrical domain was 15 cm wide and 20 cm long soil block with 2501 nodes and increased density along the upper boundary due to the tension disc infiltrometer placement. The soil hydraulic parameters (θ_r , α , n , and K_s) were initially derived from particle size distribution and bulk density data using the ROSETTA pedotransfer functions (Schaap et al., 2001) (See Table 2). The θ_r parameter was not modified, as Šimůnek et al. (1998) and González et al. (2015) found that this parameter had little effect on the simulated θ and h time series. The inverse modeling approach proposed by Šimůnek and van Genuchten (1996) was then used to calibrate α , n , and K_s in the top soil layer of each treatment starting with the initial Aeh horizon properties (Table 2).

Modeling water dynamics in the M, S and C scenarios

After performing inverse VGM parameters estimation, direct modeling was performed. Simulations included selected irrigation event (on June 24th 2014, starting 60 hours before and after irrigation was performed) in the M and S treatments during one year period (2014, on a daily time frame) in all three scenarios (M, S, and C). Simulations were performed for two-dimensional variably saturated porous media using Richards' equation:

$$\frac{\partial \theta}{\partial t} = \frac{\partial}{\partial x_i} \left[K \left(K_{ij}^A \frac{\partial h}{\partial x_j} + K_{iz}^A \right) \right] - S \quad (11)$$

where θ represents the soil volumetric water content [$L^3 L^{-3}$], h pressure head [L], x_i ($i = 1, 2$) the spatial coordinates [L], t time [T], K_{ij}^A is the components of the dimensionless hydraulic conductivity anisotropy tensor (K^A) in the two main spatial directions x_i , K is the unsaturated hydraulic conductivity [$L T^{-1}$], and S accounts for root water uptake [$L^3 L^{-3} T^{-1}$]. The root water uptake was calculated using the Feddes et al. (1978) equation. The potential root water uptake was calculated taking into account seasonal dynamics of LAI and interception of the canopy at the forest sites (beech trees). A constant rooting depth (75 cm) with a root distribution adapted from Huang et al. (2011) was assumed. Effective precipitation was further calculated by subtracting losses due to interception from gross precipitation. Seasonal variations in beech canopy were estimated using dynamic LAI with a maximum value of 5.8 and interception capacity of 2.0 mm (Armbruster et al., 2004; Breuer et al., 2003). Based on the assumptions stated above, potential root water uptake was calculated in the study of Schwen et al. (2014), performed on the same site.

The simulated domain in 2D vertical space (for specific irrigation event simulation and one year modeling) was 0.75 m deep and 2 m long (corresponding to one plot; see Figure 6 in the results section). Atmospheric boundary conditions were selected at the top and seepage conditions at the right side (down slope) to mimic the possible lateral subsurface movement as the soil profile was located on an impermeable sloped

Table 2. Van Genuchten-Mualem (VGM) soil hydraulic parameters derived from pedotransfer soil functions (PTFs, Rosetta) based on soil texture and bulk density (Table 1) with the measured saturated water content value θ_s based on evaporation experiments (Schwen et al., 2014).

Horizon	θ_r cm ³ cm ⁻³	θ_s cm ³ cm ⁻³	α cm ⁻¹	n -	K_s cm day ⁻¹	l -
Aeh	0.0433	0.47	0.026	1.4554	88.37	0.5
Bhs	0.0404	0.35	0.0335	1.4563	44.22	0.5
C	0.0391	0.32	0.0427	1.4735	36.8	0.5

bedrock. The simulation domain had 14882 nodes with the increased density at the top boundary (with 29350 2D elements). The soil layering and hydraulic properties were selected according to the Table 2, with the Aeh horizon extended to the soil surface.

Although Richards' equation is not considered applicable for hydrophobic medium (e.g., Diamantopoulos and Durner, 2013), because SWR is a reversible process and not a constant state, some of the classical physical approaches are still suitable when critical water content is exceeded.

Numerical simulations (i.e., infiltration volumes and TDR measurements) were evaluated using the coefficient of determination (R^2), root mean square error (RMSE) and model efficiency coefficient (E) (Nash and Sutcliffe, 1970):

$$R^2 = \left(\frac{\sum_{i=1}^n (O_i - \bar{O})(S_i - \bar{S})}{\sqrt{\sum_{i=1}^n (O_i - \bar{O})^2} \sqrt{\sum_{i=1}^n (S_i - \bar{S})^2}} \right)^2 \quad (12)$$

$$RMSE = \left[\frac{\sum_{i=1}^n (S_i - O_i)^2}{n} \right]^{0.5}$$

$$E = 1 - \frac{\sum_{i=1}^n (O_i - S_i)^2}{\sum_{i=1}^n (O_i - \bar{O})^2} \quad (13)$$

where O_i and S_i are observed and simulated values, respectively, \bar{O} and \bar{S} represent the averages of observed and simulated values, respectively, and n is the number of observed/simulated points.

RESULTS AND DISCUSSION

Inverse simulations of tension disc infiltrometer data

Tension disc infiltration data were used to estimate SHP by performing inverse modeling with HYDRUS (2D/3D). Modeled data is compared with field data in Fig. 2. Water infiltration for the M and S scenarios had a very steady slow inflow rate

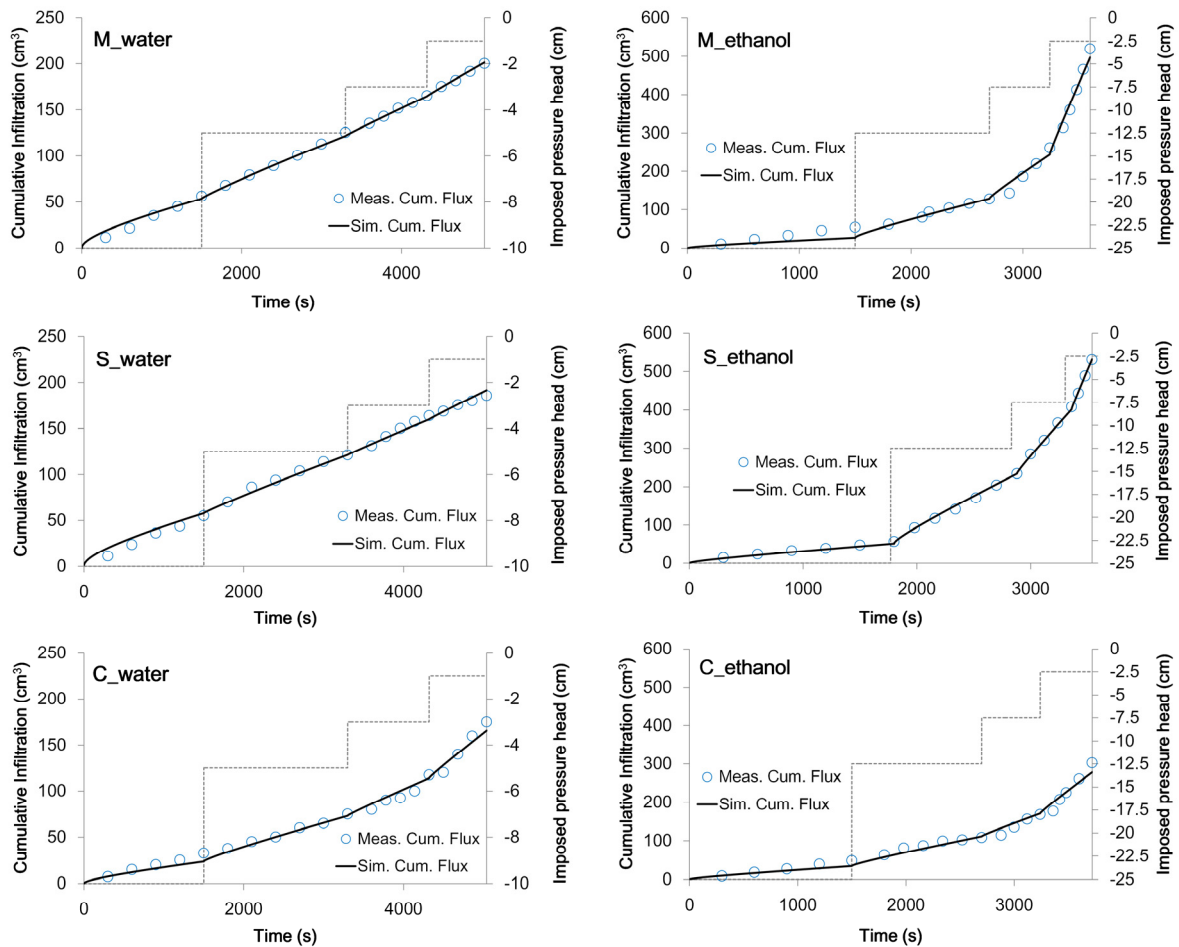
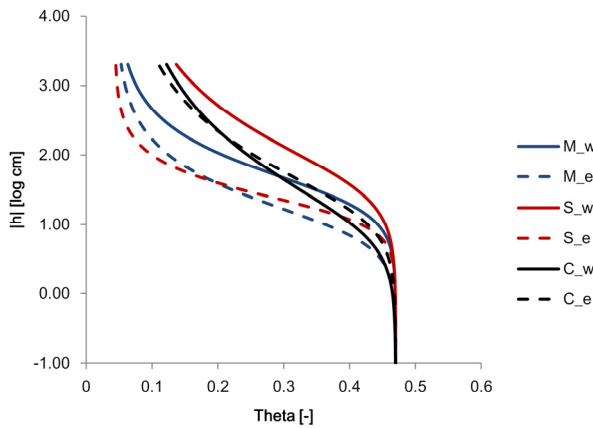


Fig. 2. Measured (circle) and simulated (solid line) infiltration cumulative fluxes for the M (moderately stressed), S (severe stressed) and C (control) scenarios with fitting performed using inverse optimization for water and ethanol liquids in HYDRUS (2D/3D) with an indication of the imposed pressure head and its duration (dotted line). Ethanol curves (_ethanol) are scaled in order to take account the different physicochemical properties and are directly comparable to water curves (_water).

Table 3. VGM parameters derived with inversion procedure using HYDRUS(2D/3D) from field infiltrometer data performed with water ($_w$) and ethanol ($_e$) liquids and statistical parameters (R^2 , E , $RMSE$) describing goodness of model fitting for Aeh horizon.

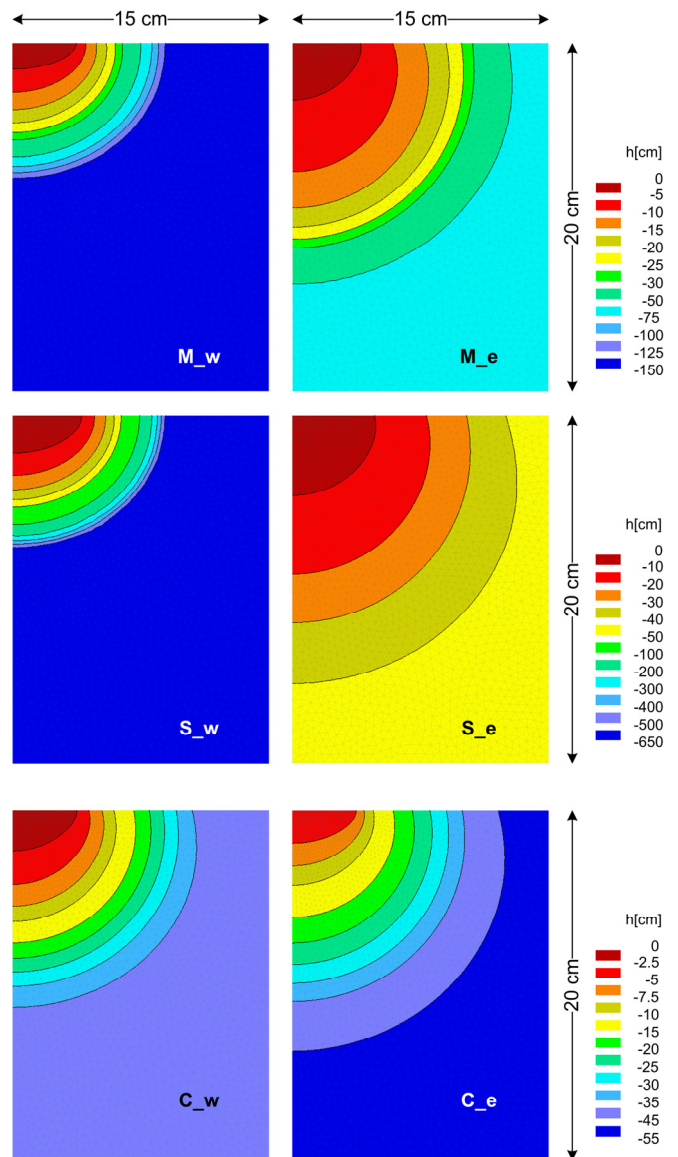
Scenario	α (cm^{-1})	n (-)	K_s cm day^{-1}	R^2	E	$RMSE$ (cm^3)
M $_w$	0.036	1.717	23.45	0.998	0.998	2.77
M $_e$	0.100	1.713	1454.26	0.981	0.985	21.6
S $_w$	0.025	1.389	27	0.995	0.995	4.14
S $_e$	0.055	2.178	440	0.999	0.999	4.25
C $_w$	0.101	1.318	257.02	0.989	0.9910	5.11
C $_e$	0.056	1.393	460.8	0.982	0.981	11.03

**Fig. 3.** Plotted retention curves for different VGM soil hydraulic parameter sets for various precipitation manipulation scenarios and different liquids (w, water vs. e, ethanol). Ethanol curves ($_e$) are scaled in order to take account the different physicochemical properties and are directly comparable to water curves ($_w$). M, moderately stressed scenario; S, severely stressed scenario; C, control scenario.

during the entire infiltration experiment and did not respond to the change in supply pressure. By contrast, a typical water infiltration curve found for non-repellent soils was observed in scenario C (although with reduced effect e.g. Šimůnek and van Genuchten, 1997), showing increased infiltration volumes at lower pressure heads (close to saturation). On the contrary, for M and S scenarios data showed reduced infiltration at lower pressure heads ($h = -3$ cm and -1 cm) and indicated that the larger pores were more hydrophobic than the smaller pores (Leue et al., 2015; Schwen et al., 2015). The final infiltration volumes were similar with 200.4, 185.7 and 175 ml for M, S and C scenarios, respectively. However, if these results are compared to the ethanol experimental data, it can be seen that the ethanol infiltration volumes are larger, with the final volumes of 519, 531 and 303 ml for M, S and C scenarios, respectively, indicating increased water repellency in the M and S scenarios. These data also show that the C scenario showed the smallest difference in total volume and infiltration curve behavior between water and ethanol. Similar results were observed by Jarvis et al. (2008) where they compared grassland to arable land with water and ethanol measurements and found that water repellency is smaller when water and ethanol infiltration volumes are similar (and *vice versa*).

The inverse optimization modeling worked well in both cases, showing a good fit for both infiltrating liquids, which can be observed visually and through statistical indicators (Fig. 2; Table 3). This shows that the VGM model describes soil hydraulic parameters well at this site. Observations through the profile indicate the presence of few macropores with a rather uniform structure (Schwen et al., 2014), suggesting that a single porosity model would be sufficient to describe the soil water

dynamics (e.g. van Genuchten, 1980). Table 3 shows a large difference between soil hydraulic properties with water and ethanol for all optimized parameters. A large increase in K_s values in the M and S scenarios was found when ethanol as a complete wetting liquid was used (Table 3) compared to water infiltration where K_s was lower. Decreases of 98.3% and 93.8% in K_s values were noticed when comparing ethanol and water infiltration for M and S scenarios. In contrast, the control scenario shows a lower increase of 44.2% compared to the water infiltration measurements. This difference also indicates that

**Fig. 4.** Pressure head distribution for M (moderately stressed) S (severely stressed) and C (control) scenarios at the end of the tension infiltration field experiment using water ($_w$) and ethanol ($_e$).

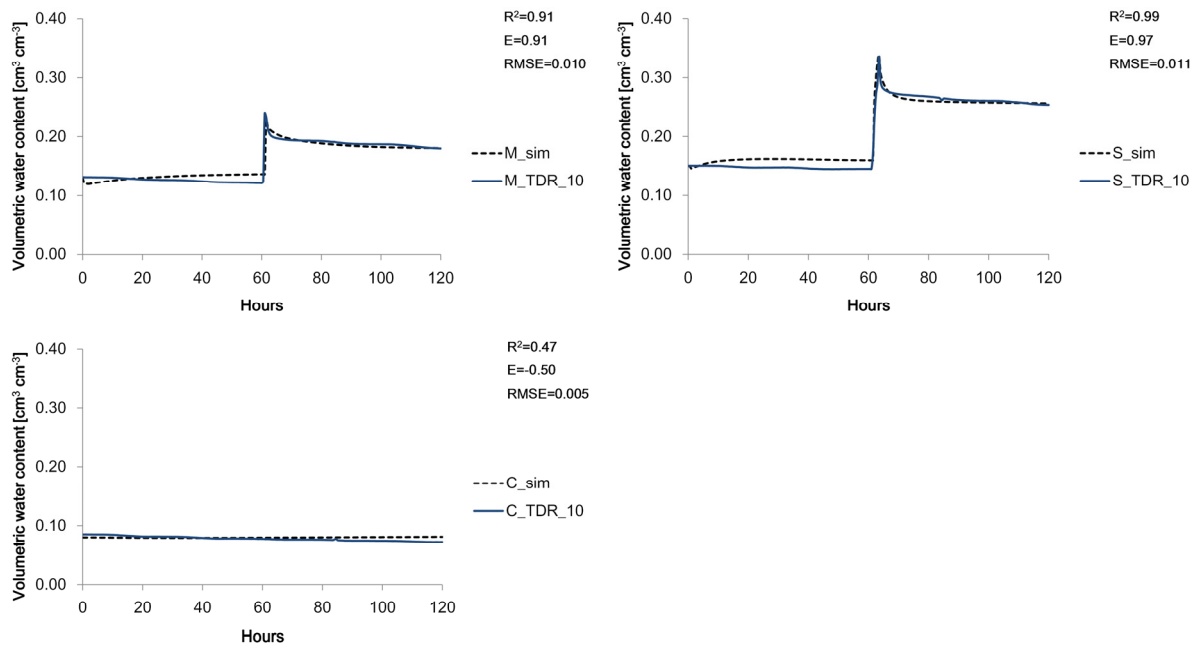


Fig. 5. Measured and simulated soil volumetric water content at 10 cm depth (Aeh horizon, TDR) using optimized parameters from water infiltration experiments from M (moderately stressed) S (severely stressed) and C (control) scenarios for the irrigation event at 24th of June 2014 (60 h before and after the event) with a 75 mm after 4 weeks of drought (M plots) and 150 mm irrigation after 8 weeks of drought (S plots) of irrigation for the event duration of 120 h.

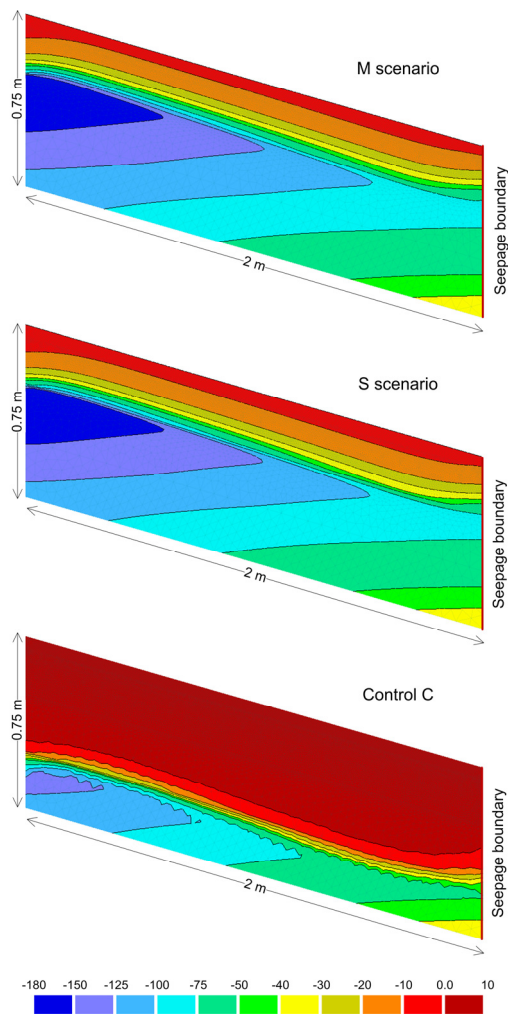


Fig. 6. Pressure head distribution for M (moderately stressed) S (severely stressed) and C (control) scenarios on the August 20th 2014 after 150 mm of the irrigation event on the previous day.

the control scenario had a certain degree of soil water repellency, which was most likely linked to the natural rainfall distribution e.g. critically low soil water content during longer periods with no rain (Schwen et al., 2015).

Fig. 3 shows fitted water retention curves based on the Table 2 parameter set for measurements derived from water (full lines) and ethanol infiltration (dotted lines). Again greater differences in the shape of the retention curve at the larger tension (drier soil condition) were recorded between the artificially induced drought stress scenarios, while the control plot had a similar shape of the retention curve for both, water and ethanol obtained SHP. It should be noted that the small differences in water retention curves of control plot might be also connected to the fitting procedure in HYDRUS since more than one set of SHP can be realistic. In addition to changes in K_s values, α and n values were increased significantly during the optimization process for ethanol data (M and S plots), resulting in a different curve shape.

Pressure head snapshots were taken at the final time of the simulated disc tension infiltration field experiment performed in HYDRUS (2D/3D) (Fig. 4). These data show that the water infiltration plume in M and S scenarios is significantly reduced compared with the ethanol infiltration plume, resulting in a very dry bottom part of the soil block (20 cm depth) even after 1.5 hours of infiltration. This part of the soil block had a pressure head of approximately -150 and -650 cm for M and S scenarios, respectively, while the ethanol treated soil had a pressure head around -75 cm. The control plot also showed differences in final pressure head values, but the lowest pressure heads were -41.58 cm for water and -54.21 cm for ethanol infiltration, respectively. The differences in duration and infiltration volumes between the two applied liquids should also be taken into consideration. Occurrence of such extensive infiltration reduction increases the risk of preferential flow in structured soils (Jarvis et al., 2008) and the potential of surface runoff as well (Cerdà and Doerr, 2007), which is further evaluated through simulations of artificially induced drought stress scenarios in the next section.

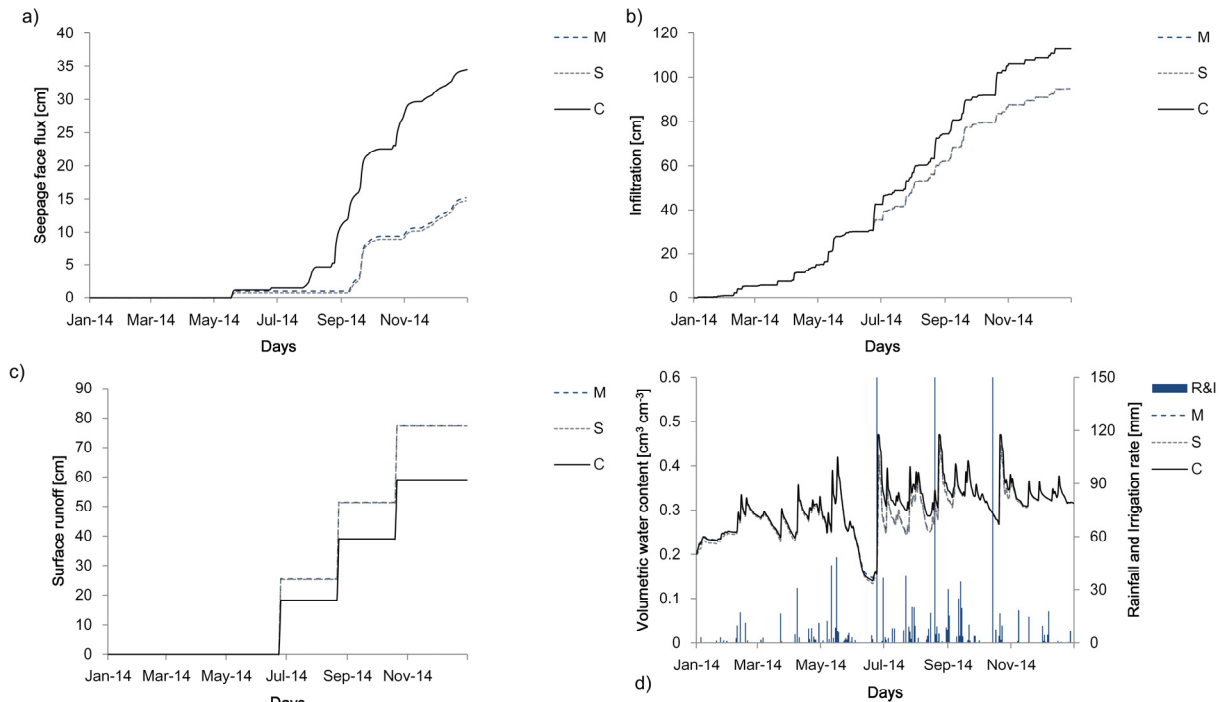


Fig. 7. Simulated cumulative seepage face flux (at the right side boundary, a), cumulative infiltration (b), cumulative runoff (c) and volumetric water content (d) at the M (moderately stressed) S (severely stressed) and C (control) scenarios during 2014 using natural rainfall and irrigation events.

Simulations of artificially induced drought stress scenarios

After the SHP were obtained by inverse modeling, a direct simulation of a particular irrigation event (on June 24th 2014) was performed for the M and S scenarios and also for the control scenario without any irrigation (Fig. 5). The selected event was simulated with a temporal resolution of 1h to provide detailed information regarding the model performance using the obtained SHP. The simulation was set to start and finish 60 hours before and after the irrigation event. Because the plots were covered during the rest of the season, simulating such shorter periods before and after the irrigation event in order to validate the model was assumed sufficient. The simulations were performed using the properties of the Aeh horizon derived from the water infiltration inverse modeling and compared to water contents measured by TDR probes at 10 cm depth (Aeh horizon) while the rest of the horizons had the same values for each layer as presented in the Table 2. Simulation of water content reproduced the field observation well with R^2 values above 0.9 and confident model efficiency values, while the model efficiency was low (-0.50) in the control scenario due to the absence of any variation during this limited period. Still, the RMSE of 0.005 indicated a good fit of the data of the control scenario. These model performance results for water content simulations are in line with previous studies using the HYDRUS model (e.g., Ajdary et al., 2007; Kandelous et al., 2011; Nakhai and Šimůnek, 2014).

Fig. 5 clearly shows a dependence between soil water content and the amount of applied irrigation water for the M and S scenarios, e.g. an instant increase of soil water content in the M scenario from 0.12 to $0.29 \text{ cm}^3 \text{ cm}^{-3}$ at the time 60.5 hours is observed, and in S scenario from 0.15 to $0.34 \text{ cm}^3 \text{ cm}^{-3}$, both corresponding to the 75 and 150 mm of irrigation, respectively. The control scenario did not show any increase in soil water content due to the absence of natural rainfall and irrigation.

After obtaining hydraulic properties from the infiltration experiment and validating the model by comparing it to field water content measurements, one year simulations were performed for 2014 using a daily time step. The simulation included plant uptake and natural rainfall and irrigation events, in order to maximize the difference between the scenarios (in terms of water balance) and to reveal potential downsides of the water repellency (e.g., surface runoff, low water content). Fig. 6 shows the pressure head distribution on August 20th, 2014 (one day after irrigation events on both irrigated plots) in the three scenarios. The differences between the scenarios are seemingly negligible for the M and S scenarios. The low conductivity of the Aeh layer ($23.45 \text{ cm day}^{-1}$ and 27 cm day^{-1} for the M and S scenario, respectively) delayed the infiltration of the irrigation plume and induced surface runoff. On the contrary, due to its non-repellent state which was expressed in larger K_s values ($257.02 \text{ cm day}^{-1}$), the irrigation plume saturated simulated profile till approximately 50 cm depth.

Our simulations suggest that in this particular case, the effect of hydrophobicity on large scale hydrology can have a substantial impact on water balance and its distribution between the infiltration and surface runoff. Fig. 7 shows differences in water balance (e.g., seepage face flux, infiltration rate and surface runoff) between artificially induced drought stress scenarios and the control plot. Due to similar SHP for the two imposed scenarios, the water balance and its distribution is almost identical. However, large seepage face flux (which in this case mimics subsurface lateral flow because of the impermeable bedrock at 75 cm) can be observed in the control plot (34.7 cm vs. 15 cm in the drought scenarios). Small K_s values in the M and S scenarios resulted in decreased infiltration and subsurface flow but increased surface runoff (77 cm in drought stress scenarios vs. 59 cm in control). The simulated water content (Fig. 7d) followed the rainfall and irrigation inputs very well and reflected the increased water levels at the top as well. The

extent of the oscillations was linked directly to the estimated SHP, e.g. a quicker response of volumetric water content changes can be seen in a control plot with the applied irrigation (simulated). Our results are in accordance with previous studies (e.g. Lemmnitz et al., 2008) which indicate that the occurrence of soil water repellency on hillslopes is important when addressing larger scale soil hydrology on a seasonal basis.

CONCLUSIONS

The HYDRUS (2D/3D) model was used to estimate soil hydraulic properties from field tension disc infiltration experiments and to quantify soil water repellency effects using data from water and ethanol infiltration measurements. Additionally, simulations to fit the TDR field moisture measurements and to perform 2D water balance modeling on an artificially induced drought stress field experiment were conducted. The water and ethanol infiltration experiments showed a large variation among the treatments and control scenario, revealing the importance of prolonged soil drying on soil water repellency. The inverse modeling was performed successfully with R^2 and model efficiency (E) values above 0.9, indicating good fit with the field measured infiltration data for both liquids (water and ethanol). Soil hydraulic properties derived from the ethanol measurements showed significantly greater K_s values for the M and S scenarios, thus suggesting linkage between water repellency and reduced infiltration. Direct simulation of irrigation events showed good reliability of the model to fit water contents measured at 10 cm depth using TDR probes. One year simulations (2014) showed that the non-structured water repellent soils have a potential to produce increased surface runoff, as well as reduced subsurface lateral flow (if impermeable or low conductivity layer is present) or vertical drainage. Climatic change scenarios are predicting more intense and prolonged droughts, as well as more extreme rainfall events, which can lead to increased soil water repellency and result in changed water flow patterns at the plot scale. Further studies are needed to clarify the occurrence, non-linear nature and impact of SWR.

Acknowledgements. This project was partly funded by the Austrian Climate and Energy Fund (ACRP 6–DRAIN–KR13AC6K11008). Sonja Leitner received a PhD fellowship of the AXA Research Fund. We also acknowledge travel funding from the bilateral agreement project HR20/2016 funded by the Austrian Agency for International Cooperation in Education (OeAD) and the Ministry of the Science and Education of the Republic of Croatia.

REFERENCES

Ajdary, K., Singh, D.K., Singh, A.K., Khanna, M., 2007. Modelling of nitrogen leaching from experimental onion field under drip irrigation. *Agr. Water Manage.*, 89, 15–28.

Armbruster, M., Seeger, J., Feger, K.H., 2004. Effects of changes in tree species composition on water flow dynamics – model applications and their limitations. *Plant Soil*, 264, 13–24.

Bachmann, J., Deurer, M., Arye, G., 2007. Modeling water movement in heterogeneous water-repellent soil: 1. Development of a contact angle-dependent water-retention model. *Vadose Zone J.*, 6, 436–445.

Bauters, T.W.J., DiCarlo, D.A., Steenhuis, T.S., Parlange, J.-Y., 2000. Soil water content dependent wetting front characteristics in sands. *J. Hydrology*, 231–232, 244–254.

Breuer, L., Eckhardt, K., Frede, H.G., 2003. Plant parameter values for models in temperate climates. *Ecol. Model.*, 169, 237–293.

Bughici, T., Wallach, R., 2016. Formation of soil-water repellency in olive orchards and its influence on infiltration pattern. *Geoderma*, 262, 1–11.

Cerdà, A., Doerr, S.H., 2007. Soil wettability, runoff and erodibility of major dry-Mediterranean land use types on calcareous soils. *Hydrol. Process.*, 21, 17, 2325–2336.

Chau, H.W., Biswas, A., Vujanovic, V., Si, B.C., 2014. Relationship between the severity, persistence of soil water repellency and the critical soil water content in water repellent soils. *Geoderma*, 221–222, 113–120.

Clothier, B.E., Vogeler, I., Magesan, G.N., 2000. The breakdown of water repellency and solute transport through a hydrophobic soil. *J. Hydrol.*, 231–232, 255–264.

Czachor, H., Doerr, S.H., Lichner, L., 2010. Water retention of repellent and subcritical repellent soils: new insights from model and experimental investigations. *J. Hydrol.*, 380, 104–111.

Debano, L.F., 1975. Infiltration, evaporation, and water movement as related to water repellency 1. In: Gardner, W.R., Moldenhauer, W.C. (Eds.): *Soil Conditioners*. SSSA Spec. Publ. 7. SSSA, Madison, WI, pp. 155–164.

Dekker, L.W., Ritsema, C.J., 1994. How water moves in a water repellent sandy soil, 1. Potential and actual water repellency. *Water Resour. Res.*, 30, 2507–2517.

Diamantopoulos, E., Durner, W., 2013. Physically-based model of soil hydraulic properties accounting for variable contact angle and its effect on hysteresis. *Adv. Water Resour.*, 59, 169–180.

Diamantopoulos, E., Durner, W., Reszkowska, A., Bachmann, J., 2013. Effect of soil water repellency on soil hydraulic properties estimated under dynamic conditions. *J. Hydrol.*, 486, 175–186.

Doerr, S.H., Shakesby, R.A., Walsh, R.P.D., 2000. Soil water repellency: its causes, characteristics and hydrogeomorphological significance. *Earth Sci. Rev.*, 51, 33–65.

Feddes, R.A., Kowalik, P.J., Zaradny, H., 1978. *Simulation of Field Water Use and Crop Yield*. John Wiley & Sons, New York.

Fischer, E.M., Knutti, R., 2014. Detection of spatially aggregated changes in temperature and precipitation extremes. *Geophys. Res. Lett.*, 41, 2, 547–554.

Ganz, C., Bachmann, J., Noell, U., Diujnisveld, W.H.M., Lamparter, A., 2014. Hydraulic modeling and in situ electrical resistivity tomography to analyze ponded infiltration into a water repellent sand. *Vadose Zone J.*, 13, 1, 1–14.

Gee, G.W., Or, D., 2002. Particle-size analysis. In: Dane, J.H., Topp, G.C. (Eds.): *Methods of Soil Analysis*. Part 4 – Physical Methods. SSSA Book Series, No. 5. SSSA, Madison, WI, USA, pp. 1381–1402.

González, M.G., Ramos, T.B., Carlesso, R., Paredes, P., Petry, M.T., Martins, J.D., Aires, N.P., Pereira, L.S., 2015. Modelling soil water dynamics of full and deficit drip irrigated maize cultivated under a rain shelter. *Biosyst. Eng.*, 132, 1–18. DOI: 10.1016/j.biosystemseng.2015.02.001.

Hallett, P.D., Baumgartl, T., Young, I.M., 2001. Subcritical water repellency of aggregates from a range of soil management practices. *Soil Sci. Soc. Am. J.*, 65, 184–190.

Hardie, A.H., Lisson, S., Doyle, R.B., Cothing, W.E., 2013. Evaluation of rapid approaches for determining the soil water retention function and saturated hydraulic conductivity in a hydrologically complex soil. *Soil Till. Res.*, 130, 99–108.

- Hopmans, J.W., Šimůnek, J., Romano, N., Durner, W., 2002. Inverse methods. In: Dane, J.H., Topp, G.C. (Eds.): *Methods of Soil Analysis. Part 4. SSSA Book Series, No. 5.* SSSA, Madison, WI, pp. 963–1008.
- Huang, M., Barbour, S.L., Elshorbagy, A., Zettl, J.D., Si, B.C., 2011. Water availability and forest growth in coarse-textured soils. *Canad. J. Soil Sci.*, 91, 199–210.
- IUSS, 2014. World reference base for soil resources. FAO, Rome.
- Jarvis, N., Etana, A., Stagnitti, F., 2008. Water repellency, near-saturated infiltration and preferential solute transport in a macroporous clay soil. *Geoderma*, 143, 223–230.
- Jordán, A., Zavala, L.M., Mataix-Solera, J., Doerr, S.H., 2013. Soil water repellency: origin, assessment and geomorphological consequences. *Catena*, 108, 1–5.
- Kandelous, M.M., Šimůnek, J., van Genuchten, M.Th., Malek, K., 2011. Soil water content distributions between two emitters of a subsurface drip irrigation system. *Soil Soil Sci. Soc. Am. J.*, 75, 488–497.
- Lamparter, A., Bachmann, J., Deurer, M., Woche, S.K., 2010. Applicability of ethanol for measuring intrinsic hydraulic properties of sand with various water repellency levels. *Vadose Zone J.*, 9, 445–450.
- Leitner, S., Minixhofer, P., Inselsbacher, E., Keiblinger, K.M., Zimmermann, M., Zechmeister-Boltenstern, S., 2017. Short-term soil mineral and organic nitrogen fluxes during moderate and severe drying-rewetting events. *Appl. Soil Ecol.*, 114, 28–33.
- Lemnitz, C., Kuhnert, M., Bens, O., Güntner, A., Merz, B., Hüttl, R.F., 2008. Spatial and temporal variations of actual soil water repellency and their influence on surface runoff. *Hydrol. Process.*, 22, 1976–1984.
- Lenhard, R.J., Parker, J.C. 1992. Modeling multiphase fluid hysteresis and comparing results to laboratory investigations. In: Genuchten, M.Th., Leij, F.J., Lund, L.J. (Eds.); *Proc. Intl. Workshop on Indirect Methods for Estimating the Hydraulic Properties of Unsaturated Soils.* University of California, Riverside, CA.
- Letey, J., Carrillo, M.L.K., Pang, X.P., 2000. Approaches to characterize the degree of water repellency. *J. Hydrol.*, 231–232, 61–65.
- Leue, M., H.H. Gerke, Godow, S.C., 2015. Droplet infiltration and organic matter composition of intact crack and biopore surfaces from clay-illuvial horizons. *J. Plant Nutr. Soil Sci.*, 178, 250–260.
- Liu, H., Ju, Z., Bachmann, J., Horton, R., Ren, T., 2012. Moisture-dependent wettability of artificial hydrophobic soils and its relevance for soil water desorption curves. *Soil Sci. Soc. Am. J.*, 76, 342–349.
- Monteith, J.L., 1981. Evaporation and surface temperature. *Q. J. R. Meteorol. Soc.*, 107, 1–27.
- Mualem, Y., 1976. A new model for predicting the hydraulic conductivity of unsaturated porous media. *Water Resour. Res.*, 12, 3, 513–521.
- Nakhaei, M., Šimůnek, J., 2014. Parameter estimation of soil hydraulic and thermal property functions for unsaturated porous media using the HYDRUS-2D code. *J. Hydrol. Hydro-mech.*, 62, 7–15.
- Nash, J.E., Sutcliffe, J.V., 1970. River flow forecasting through conceptual models. Part I. A discussion of principles. *J. Hydrol.*, 10, 282–90.
- Nieber, J., Bauters, T.W.J., Steenhuis, T.S., Parlange, J.Y., 2000. Numerical simulation of experimental gravity-driven unstable flow in water repellent sand. *J. Hydrol.*, 231–232, 295–307.
- Ritsema, C.J., Dekker, L.W., 2000. Preferential flow in water repellent sandy soils: principles and modeling implications. *J. Hydrol.*, 231–232, 308–319.
- Ritsema, C., Dekker, L.W., Hendrickx, J.M.H., Hamminga, W., 1993. Preferential flow mechanism in a water repellent sandy soil. *Water Resour. Res.*, 29, 2183–2193.
- Schaap, M.G., Leij, F.J., van Genuchten, M.T., 2001. ROSET-TA: a computer program for estimating soil hydraulic parameters with hierarchical pedotransfer functions. *J. Hydrol.*, 251, 163–176.
- Schindler, U., Durner, W., von Unold, Georg., Müller, L., 2010. Evaporation method for measuring unsaturated hydraulic properties of soils: extending the measurement range. *Soil Sci. Soc. Am. J.*, 74, 1071–1083.
- Schwen, A., Zimmermann, M., Bodner, G., 2014. Vertical variations of soil hydraulic properties within two soil profiles and its relevance for soil water simulations. *J. Hydrol.*, 516, 169–181.
- Schwen, A., Zimmermann, M., Leitner, S., Woche, S.K., 2015. Soil Water Repellency and its Impact on Hydraulic Characteristics in a Beech Forest under Simulated Climate Change. *Vadose Zone J.*, 14, 12, 1–11.
- Shang, J., Flury, M., Harsh, J.B., Zollars, R.L., 2008. Comparison of different methods to measure contact angles of soil colloids. *J. Colloid Interface Sci.*, 328, 299–307.
- Šimůnek, J., van Genuchten, M.Th., 1996. Estimating unsaturated soil hydraulic properties from tension disc infiltrometer data by numerical inversion. *Water Resour. Res.*, 32, 2683–2696.
- Šimůnek, J., van Genuchten, M.Th., 1997. Parameter estimation of soil hydraulic properties from multiple tension disc infiltrometer data. *Soil Sci.*, 162, 383–398.
- Šimůnek, J., Angulo-Jaramillo, R., Schaap, M.G., Vandervaere, J.P., van Genuchten, M.T., 1998. Using an inverse method to estimate the hydraulic properties of crusted soils from tension disc infiltrometer data. *Geoderma*, 86, 61–81.
- Šimůnek, J., van Genuchten, M.Th., Šejna, M., 2016. Recent developments and applications of the HYDRUS computer software packages. *Vadose Zone J.*, 15, 7. DOI: 10.2136/vzj2016.04.0033
- Stocker, T.F., Qin, D., Plattner, G.-K., Tignor, M.M.B., Allen, S.K., Boschung, J., Nauels, A., Xia, Y., Bex, V., Midgley, P.M. (Eds.), 2013. *Climate Change. The Physical Science Basis. Summary for Policymakers.* Working Group I Contribution to the Fifth Assessment Report of the Intergovernmental Panel on Climate Change. Cambridge Univ. Press, Cambridge and New York, pp. 1–30.
- Stoffregen, H., Wessolek, G., 2014. Scaling the hydraulic functions of a water repellent sandy soil. *Int. Agrophys.*, 28, 349–358.
- Subedi, S., Kawamoto, K., Komatsu, T., Moldrup, P., Wollesen de Jonge, L., Müller, K., Clothier, B., 2013. Contact angles of water-repellent porous media inferred by tensiometer-TDR probe measurement under controlled wetting and drying cycles. *Soil Sci. Soc. Am. J.*, 77, 1944–1954.
- van Genuchten, M.Th., 1980. A closed-form equation for predicting the hydraulic conductivity of unsaturated soils. *Soil Sci. Soc. Am. J.*, 44, 892–898.
- Vereecken, H., Schnepf, A., Hopmans, J.W., Javaux, M., Or, D., Roose, T., Vanderborght, J., Young, M.H., Amelung, W., Aitkenhead, M., Allison, S.D., Assouline, S., Baveye, P., Berli, M., Brüggemann, N., Finke, P., Flury, M., Gaiser, T., Govers, G., Ghezzehei, T., Hallett, P., Hendricks Franssen, H.J., Heppell, J., Horn, R., Huisman, J.A., Jacques, D., Jonard, F., Kollet, S., Lafolie, F., Lamorski, K., Leitner,

D., McBratney, A., Minasny, B., Montzka, C., Nowak, W., Pachepsky, Y., Padarian, J., Romano, N., Roth, K., Rothfuss, Y., Rowe, E.C., Schwen, A., Šimůnek, J., Tiktak, A., Van Dam, J., van der Zee, S.E.A.T.M., Vogel, H.J., Vrugt, J.A., Wöhling, T., Young, I.M., 2016. Modeling soil processes:

Review, key challenges, and new perspectives. *Vadose Zone J.*, 15, 5. DOI: 10.2136/vzj2015.09.0131.
Watson, C.L., Letey, J., 1970. Indices for characterizing soil-water repellency based upon contact angle-surface tension relationships. *Soil Sci. Soc. Am. Proc.*, 34, 841–844.

Received 17 July 2017
Accepted 29 December 2017

Note: Colour version of Figures can be found in the web version of this article.